A Method to Estimate Residual Stress in Austenitic Stainless Steel Using a Microindentation Test

Akio Yonezu, Ryota Kusano, Tomohiro Hiyoshi, and Xi Chen

This study proposed a method to evaluate the residual stress and plastic strain of an austenitic stainless steel using a microindentation test. The austenitic stainless steel SUS316L obeys the Ludwick's work hardening law and is subjected to in-plane equi-biaxial residual stress. A numerical experiment with the finite element method (FEM) was carried out to simulate an indentation test for SUS316L having various plastic strains (pre-strains) and residual stresses. It was found that the indentation force increased with increasing pre-strain as well as with compressive residual stress. Next, a parametric FEM study by changing both residual stress σ_{res} and pre-strain ε_{pre} was conducted to deduce the relationship between the indentation curve and the parameters ε_{pre} and σ_{res} (which were employed for the FEM study). This relationship can be expressed by a dimensionless function with simple formulae. Thus, the present method can estimate both ε_{pre} and σ_{res}, when a single indentation test is applied to SUS316L.

1. Introduction

Development of residual stresses is often experienced in engineering steels due to inhomogeneous strain distribution and mechanical constraints. Residual stresses are produced due to many reasons. For instance, residual stress is formed when a material undergoes inhomogeneous plastic deformation due to plastic work (i.e., cold working and sheet forming) and surface treatments/modifications (Ref 1, 2). In particular, tensile residual stress induces environmental-assisted cracking and fatigue crack initiation, resulting in severe damage (Ref 3, 4). Thus, the evaluation of residual stress is very important for industrial steels and structures. For such a case, residual strains caused by local plastic deformation (pre-plastic strain) may be an important issue as it is related to the development of residual stress. In other words, local and inhomogeneous plastic strain induces mechanical constraint, resulting in the development of residual stresses. Therefore, an evaluation of both residual stress and plastic strain may be required to maintain the integrity of a material as well as to design materials and structures. X-ray diffraction is widely used to measure residual stress. This method has been fully developed and is often employed in field inspections. However, a particular crystalline structure (i.e., grain coarsening and crystal texture) may make accurate measurements difficult (Ref 5), and it is not suitable for small material structures. In addition, the x-ray diffraction method cannot evaluate plastic strain (called pre-strain), which is often coupled with the level of residual stress.

Instrumented indentation technique is a convenient process to determine mechanical properties, including Young's modulus and hardness (Ref 6, 7). Furthermore, elastoplastic properties (i.e., uniaxial stress-strain curve) can be derived from the experimental data of an indentation curve, which represents the relationship between indentation force and penetration depth, and an impression (residual imprint) (Ref 8-10). In these studies, the dimensional function that correlates the parameters of indentation responses (mostly the indentation curve) with the elastoplastic properties of a material is first established through a forward analysis (indentation responses obtained from material properties) using computational approaches (Ref 11-13). The elastoplastic properties can then be identified, when the experimentally obtained indentation responses are assigned to the function (i.e., reverse analysis: material properties identified from indentation responses). Thus, this method may evaluate the plastic strain due to plastic deformation when the estimated stress-strain curve matches with that of the undeformed material (Ref 14). In fact, it is well known that work hardening due to plastic deformation increases the hardness of a material (Ref 6, 15-17). Therefore, the indentation technique is useful for measuring local elastoplastic properties, including the plastic strain.

Several other attempts to evaluate the residual stress based on an indentation test were proposed in previous studies. For example, Suresh and Giannakopoulos (Ref 18) focused on the change of impressions due to residual stress, and their relationship was investigated by an analytical formula. This was based on the findings of Tsui et al. (Ref 19). However, the influence of residual stress on an impression may be relatively small to be measured experimentally. Thus, it is not clear whether the method can be practically applied except when the residual stress is large (near the yield stress). Swadener et al. (Ref 20) proposed a simple approach based on the depth-sensing indentation test.

Akio Yonezu, Ryota Kusano, and **Tomohiro Hiyoshi**, Department of Precision Mechanics, Chuo University, 1-13-27 Kasuga, Bunkyo, Tokyo 112-8551, Japan; and **Xi Chen**, Department of Earth and Environmental Engineering, Columbia University, 500 W 120th Street, New York, NY 10027 and International Center for Applied Mechanics, SV Lab, School of Aerospace, Xi'an Jiaotong University, Xi'an 710049, China. Contact e-mails: yonezu@mech.chuo-u.ac.jp and xichen@columbia.edu.

Table 1 Mechanical properties of austenitic stainless steel (SIS316L) employed in this study

Young's modulus E, GPa	Poisson's ratio v	Yield stress σ_Y, GPa	Work hardening exponent n	Work hardening strength K, GPa
195	0.3	0.260	0.70	1.19

Their method may be useful, when an intermediate indentation force is used since the transition regime between elastic and plastic contact (i.e., elastic-plastic transition) is greatly affected by the residual stress. Xu et al. (Ref 21) proposed a similar idea with a flat punch indenter. Those challenges were reported in a review article (Ref 22). However, in order to apply those methods with a general indentation force, precise depth measurements may be required. In addition, yield strength (plastic properties) should be known prior to the estimation of residual stress. As mentioned previously, simultaneous evaluations of both plastic strain (plastic properties including yield stress) and residual stress are also required through an indentation method, which we understand to still be an open research topic.

Other methods have been proposed in the literature. For example, inverse analysis methods were established to evaluate the residual stress from an indentation curve (Ref 23, 24). These methods can also evaluate other unknown mechanical properties, such as Young's modulus and yield stress. However, these methods require a great deal of effort and have not found widespread use, since the estimation procedure requires iterative FEM computations (forward analysis) with, for example, an optimization algorithm (Ref 23) and an updating response surface (Ref 24). When a method is required for practical situations, reverse analysis based on a simple framework (without special computational requirements) is more desirable. For instance, Chen et al. proposed a reverse analysis technique based on an indentation curve in order to estimate the elastoplastic property and residual stress (Ref 25, 26). This method is reliable, but there are some issues. For instance, the range of materials application is very limited (i.e., no work hardening), and complex functions are used.

This study proposes a simple method to evaluate both residual stress and plastic strain (plastic properties)* using a new indentation method. Since this study is the first step to establish such a simple evaluation framework, we focus only on austenitic stainless steel (SUS316L) having equi-biaxial residual stress. In fact, stainless steel is commercially available, and is widely used in industrial mechanical components and chemical/electronic power plants. In chemical plants, the steel often suffers from mechanical degradation (fatigue and stress corrosion cracking, SCC) due to tensile residual stress. To prevent such issues, compressive residual stresses are usually introduced via a peening technique. This technique may introduce equi-biaxial compressive stress on the material surface. By considering such an engineering background, this study focuses on SUS316L having equi-biaxial residual stress and plastic strain. In other words, it aims to establish reverse analysis with a simple framework to simultaneously evaluate residual stress and plastic strain in SUS316L. In this research, reverse analysis is established via a parametric study using a finite element method (FEM). Our method is subsequently verified by computational and experimental data. Some issues and future challenges are also discussed.

---

*Residual stress and plastic strain are not "material properties", but are "mechanical preparing conditions" instead. This study aims to evaluate those two parameters using a single indentation test.
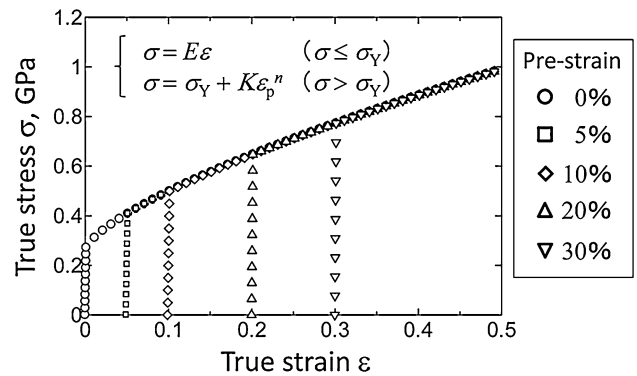

Fig. 1 True stress-strain curve of austenitic stainless steel with various pre-strains

2. Materials

The material considered in this study is austenitic stainless steel (SUS316L) and its mechanical properties are listed in Table 1. These properties were obtained from a uniaxial tensile test of as-received SUS316L (which is commercially available) (Ref 14). The true stress and true strain curve in the plastic region can be approximated by Ludwick's law (Ref 14). The constitutive equation in the elastic and plastic region is described as follows:

$$\sigma = E\varepsilon \quad \text{for} \quad \sigma \leq \sigma_Y \quad \text{and} \quad \sigma = \sigma_Y + K\varepsilon_p^n$$
$$\text{for} \quad \sigma \geq \sigma_Y, \tag{Eq 1}$$

where E is the Young's modulus, σ_Y is the yield stress, n is the work hardening exponent, and K is the work hardening strength. Note that ε_p is plastic strain. The stress-strain curve of SUS316L is shown in Fig. 1. The curve is expressed by Eq 1 and Table 1.

We next considered the plastically deformed steel. This study assumed that when the steel experiences plastic strain due to plastic deformation, the stress-strain data correspond to the curve of the as-received steel by shifting of the applied plastic strain. This example is also shown in Fig. 1, indicating pre-strains of 5, 10, 20, and 30%. In other words, the yield stress of pre-strained steel increased due to work hardening, which was then plotted on the stress-strain curve of as-received steel when it shifted to the value of pre-strain. In fact, this phenomenon was observed, when uniaxial loading was applied to the as-received steel and pre-strained steel (Ref 15, 17). Cyclic plastic deformation along one direction may show a similar trend. However, the increase of yield stress due to work hardening depends on the loading direction. This is well known to be Baushinger effect, and cyclic plastic deformation obeys the kinematic hardening rule. For simplicity, this study assumed that the effect of loading direction of plastic deformation is negligible. In other words, the material obeys the isotropic hardening rule. It was also assumed that the elastic modulus does not change even if the steel undergoes plastic deformation (i.e., the pre-strain is introduced in the steel).

Since this study addresses only SUS316L, the yield stress of pre-strained steel can be expressed by substituting pre-strain into Eq 1. In fact, Fig. 1 shows the stress-strain curves of pre-strained steels having different pre-strain values (5, 10, 20, and 30%) obtained using Eq 1. Therefore, the plastic properties can be expressed by only the parameter of pre-strain ε_{pre}. The yield stress σ_Y can be obtained from Fig. 1, when the pre-strain value is known.

On the contrary, residual stress is assumed to be introduced equi-biaxially on the specimen surface. The stress component is considered to be both tension and compression. Therefore, this study will evaluate pre-strain (plastic strain) and residual stress of stainless steel.

3. Numerical Analysis

3.1 Model Definition

Figure 2 shows the schematic of an indentation test using a conical sharp indenter. As a typical sharp indenter, the Berkovich indenter is widely used. The indenter has a triangular shape with a diagonal angle of 115°. For the simplicity of computations and to approximate an axisymmetric model, this study used a conical indenter as shown in Fig. 2(a). The half apex angle α is 70.3°, so that the contact area as a function of indentation depth equals between the two (for a Berkovich indenter and conical indenter).

In Fig. 2(a), the indenter penetrates the material surface for a given maximum indentation force F_{max}, to a certain penetration depth, which is designated by the maximum indentation depth h_{max}. Note that the indenter penetrates into the region that experiences full plastic deformation. Subsequently, the indenter is withdrawn, such that the maximum force drops to zero. Following this full unloading, a permanent impression (crater) is observed. The residual depth is described by h_r in Fig. 2(a). Such a loading and unloading cycle is shown in Fig. 2(b), where the material locally deforms elastically and plastically during the loading, and then recovers elastically during the unloading. In this figure, the area of indentation curve corresponds to a total work volume W** due to indenter penetration. Contrary to this, the area corresponding to the unloading (as shown by the blue shaded area, W_u) indicates the work of elastic recovery (unloading work). Here, the recovery depth h_e can be obtained by $h_{max} - h_r$. Consequently, the total work, $W = \int_0^{h_{max}} F dh$ and the unloading work, $W_u = -\int_{h_{max}}^{h_r} F dh$ can be obtained.

Figure 2(c) shows the schematic of in-plane residual stress σ_{res} which is introduced in the material. This study focuses on the equi-biaxial residual stress with both compression and tension.

3.2 Finite Element Method

The axi-symmetric model of the two-dimensional (2D) FEM was created to compute the response of the indentation test, as shown in Fig. 3. The model comprises about 20,000 four-node elements, wherein fine meshes were created around the contact region, and a mesh converge test was carried out. The conical indenter whose half apex angle is 70.3° was employed for the 2D model using the Berkovich indenter (as mentioned above).

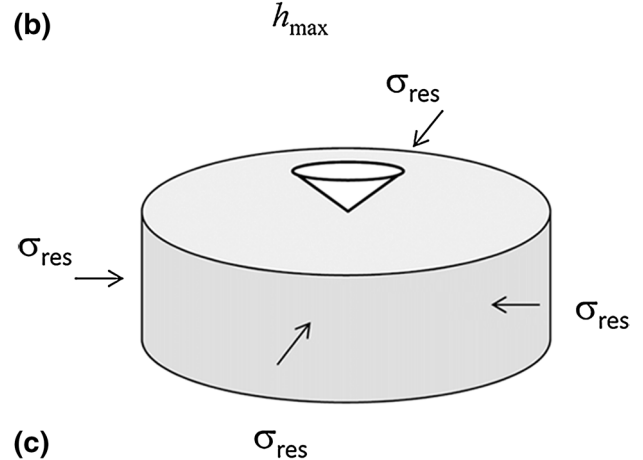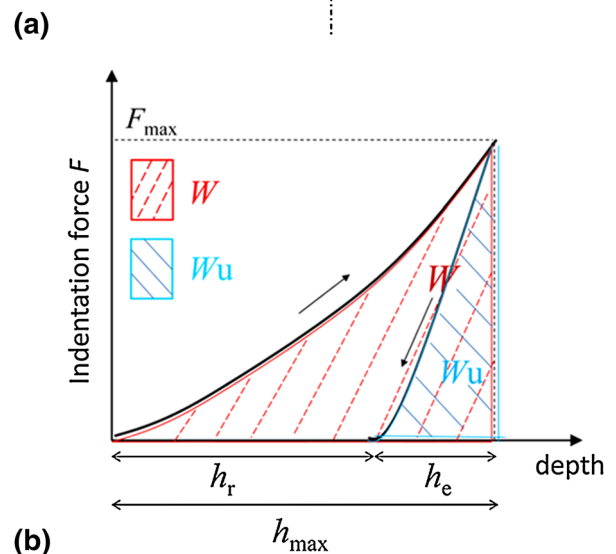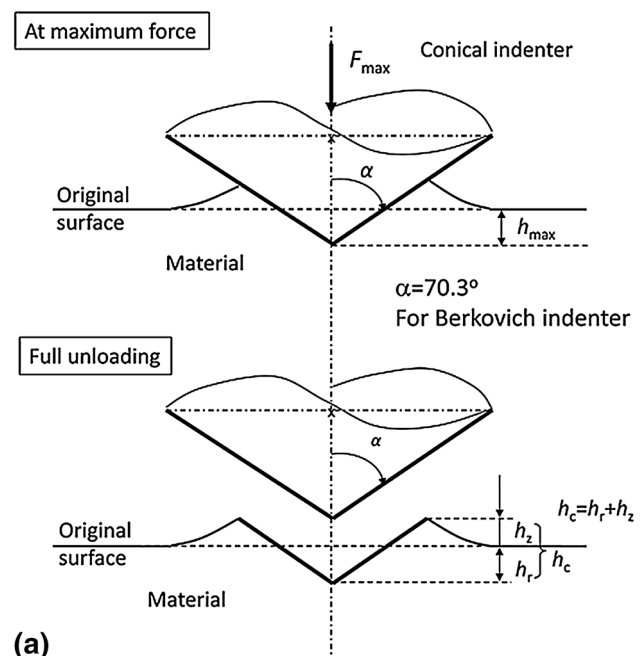**This is also called "indentation energy".

(a)

(b)

(c)

Fig. 2   (a) Schematic of indentation loading and unloading; (b) definition of work volume in the indentation curve; and (c) residual stress state during indentation loading

In the FEM model, the indenter is assumed a rigid body. The indenter penetrates up to 10 μm into the material and is withdrawn until completely unloaded.
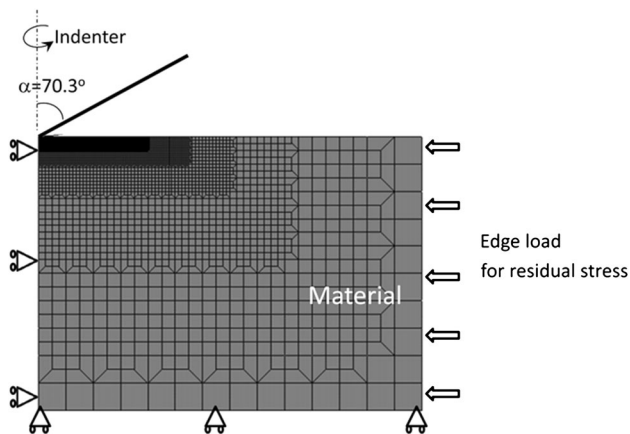
Fig. 3 Axi-symmetric two-dimensional FEM model for Berkovich indentation

Fig. 4 Indentation curves of the as-received SUS316L determined by the FEM computation (circles) and experiment (solid line)

Computations were carried out using a commercially available software, Marc (Ref 27). Coulomb's law of friction was assumed, and a coefficient of friction of $\nu = 0.15$ was used, which is often regarded as a minor influence in indentation analysis (Ref 13, 28). In addition, the Poisson's ratio was set to 0.3 for all computations. As shown in Table 1, Young's modulus E was set to 195 GPa. Referring to Eq 1, this study employed various plastic properties, which can be expressed by the plastic strain (pre-strain, ε_{pre}) as described in Fig. 1. As shown in this figure, the yield stress σ_Y increases with an increase in pre-strain, indicating that σ_Y is uniquely dependent on pre-strain ε_{pre}. Thus, the yield stress present is described by $\sigma_{Y(\varepsilon pre)}$ hereafter. The pre-strain ε_{pre} values employed were 0, 5, 10, 20, 30, 40, 60, and 100%[†]. A pre-strain ε_{pre} of 0% corresponds to the as-received virgin material as shown in Table 1. This study conducted an elastoplastic analysis with the von Mises yield criterion.

In order to introduce the in-plane residual stress, a mechanical loading (edge loading) was applied to the material from the side surface as shown in Fig. 3. Since the model size was relatively large with a depth of 8.4 mm and a radius of 20.4 mm, the effect of boundary conditions due to edge loading on the indentation response could be ignored. Therefore, the residual stress was uniformly introduced to the material. This study introduced various residual stresses σ_{res} in the material before indenter penetration (indentation loading). Note that σ_{res} normalized by $\sigma_{Y(\varepsilon pre)}$ ($\sigma_{res}/\sigma_{Y(\varepsilon pre)}$) was used for the assigned parameter in the parametric FEM study. The value of $\sigma_{res}/\sigma_{Y(\varepsilon pre)}$ varied among -0.75, -0.25, 0, $+0.25$, and $+0.75$. Thus, the eight total pre-strain values and the five total $\sigma_{res}/\sigma_{Y(\varepsilon pre)}$ values gave rise to 40 total computations during the course of this study.

3.3 Representative Computational Results

To verify our FEM model, a preliminary computation for the as-received steel was carried out. The computed indentation curve is shown in Fig. 4. This was compared to the experimental data, and as can be seen, both curves show good agreement with each other.

[†]In fact, a pre-strain of 100% in compression is not realistic, but the present study considers the von Mises yield criterion, and von Mises stress is employed as described in Eq 1. Note that a pre-strain of 100% is the limitation of our method.
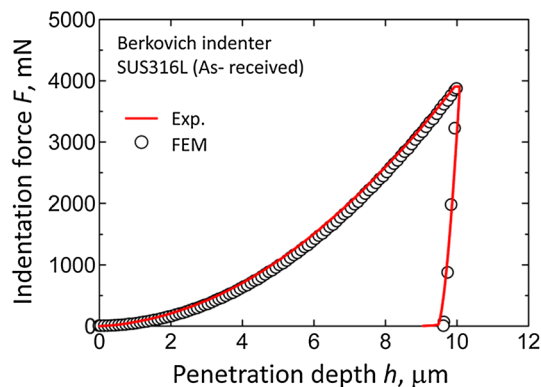
This study next investigated the effect of pre-strain and residual stress on the indentation curve. Figure 5 shows the indentation curves, indicating the dependence of pre-strain (Fig. 5a) and that of residual stress ($\sigma_{res}/\sigma_{Y(\varepsilon pre)}$, in Fig. 5b). In Fig. 5(a), the result of no residual stress shows that the indentation force increases as ε_{pre} increases (owing largely to the higher yielding level). In Fig. 5(b), it is found that the indentation force increases with compressive residual stress. On the other hand, the indentation force decreases with increase in tensile residual stress. A similar trend was observed in a previous study (Ref 26). It is thus concluded that both pre-strain and residual stress affect the indentation curve. These characteristics assist in establishing the dimensionless function for reverse analysis, which will be discussed in the next section.

4. Estimation Method

4.1 Dimensionless Analysis

As mentioned above, there are many previous studies on the estimation of elastoplastic properties based on a dimensionless function (Ref 8, 12, 13, 29). Such a simple function may be useful for reverse analysis. Similarly, this study conducted a dimensionless analysis to develop the estimation method of both ε_{pre} and σ_{res}. In other words, the dimensionless function, which correlates the indentation curve with the parameters to be identified (ε_{pre} and σ_{res}), was established through the parametric FEM study. Since there are two parameters identified (ε_{pre} and σ_{res}), two independent parameters are required in an indentation curve. As shown in Fig. 2(b), the total work W and the elastic work W_u were investigated in this study, as these two parameters are independent.

The total work volume W in the indentation curve depends on the elastoplastic properties, mechanical preparation conditions (ε_{pre}, σ_{res}), and indentation testing conditions (the maximum depth h_{max} and indenter tip angle α). It can be expressed as follows:

$$W = f_1(E^*, \sigma_{res}, \varepsilon_{pre}\ \sigma_Y, n, K, h_{max}, \alpha). \tag{Eq 2}$$

As explained above, the plastic property (σ_Y, n, K) is dependent on the pre-strain ε_{pre}, and can be determined uniquely given ε_{pre} (see Fig. 1 for the fixed material investigated in the present paper). In addition, the indenter angle α is
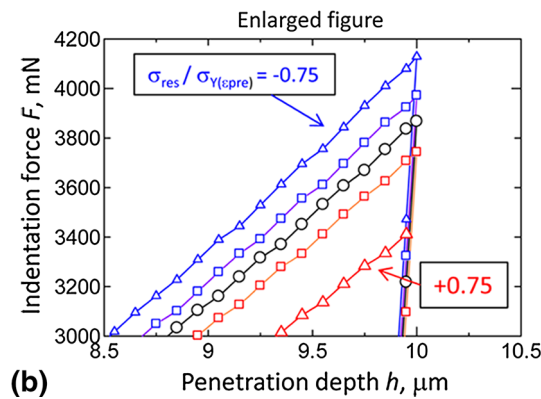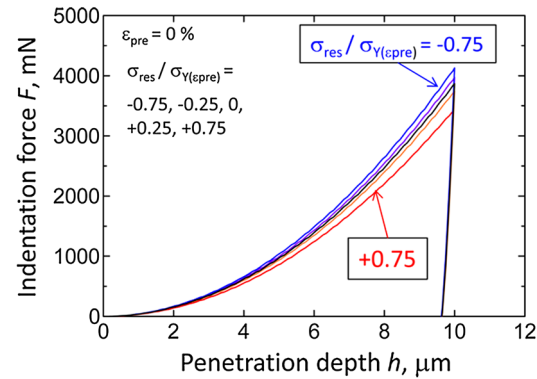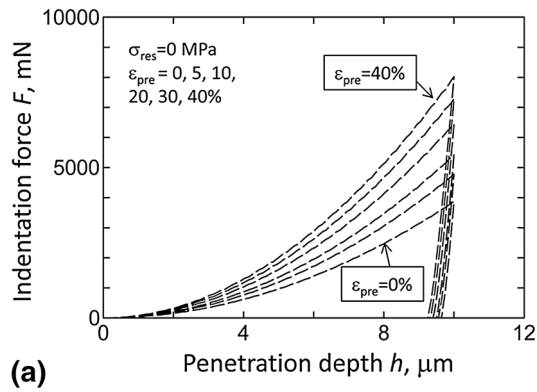
Fig. 5 Effect of pre-strain (a) and residual stress (b) on the indentation curves
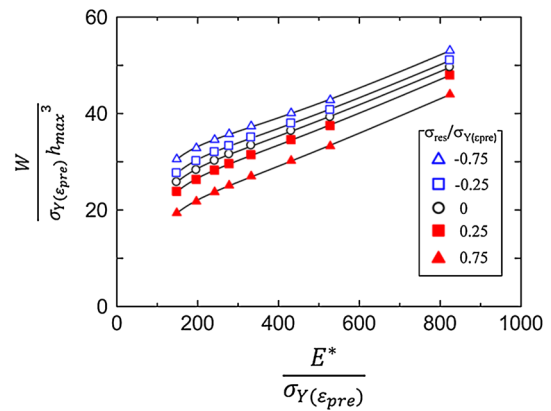

Fig. 6 Relationship between $\frac{W}{\sigma_{Y(\varepsilon pre)} h_{max}^3}$ and $\frac{E^*}{\sigma_{Y(\varepsilon pre)}}$ at each $\frac{\sigma_{res}}{\sigma_{Y(\varepsilon pre)}}$

fixed and can be removed from the current function. Thus, Eq 2 can be simplified using $\sigma_{Y(\varepsilon pre)}$ as follows:

$$W = f_1(E^*, \sigma_{res}, \sigma_{Y(\varepsilon pre)}, h_{max}). \qquad (Eq\ 3)$$

In this study, $\sigma_{Y(\varepsilon pre)}$ and h_{max} were varied to investigate their coupled effects, and the dimensionless function with Π theory was used to obtain the following dimensionless function:

$$\frac{W}{\sigma_{Y(\varepsilon pre)} h_{max}^3} = \Pi\left(\frac{E^*}{\sigma_{Y(\varepsilon pre)}}, \frac{\sigma_{res}}{\sigma_{Y(\varepsilon pre)}}\right). \qquad (Eq\ 4)$$

Similarly, the dimensionless function of elastic work W_u (indentation unloading curve) can be obtained as follows:

$$\frac{W_u}{\sigma_{Y(\varepsilon pre)} h_e^3} = \Pi\left(\frac{E^*}{\sigma_{Y(\varepsilon pre)}}, \frac{\sigma_{res}}{\sigma_{Y(\varepsilon pre)}}\right). \qquad (Eq\ 5)$$

Here, the yield stress $\sigma_{Y(\varepsilon pre)}$ is related to pre-strain ε_{pre} via Eq 1 (see Fig. 1). In both Eq 4 and 5, E^* is the reduced

Young's modulus, which can be expressed by $\frac{1}{E^*} = \left(\frac{1-v_s^2}{E_s} + \frac{1-v_i^2}{E_i}\right)$. Note that the subscripts "s" and "i" denote "specimen" and "indenter", respectively.

The data of the parametric FEM study on the 40 cases spanning the material parameter space were introduced into Eq 4, and the results are shown in Fig. 6. The values of $\frac{W}{\sigma_{Y(\varepsilon pre)} h_{max}^3}$ increase in $\frac{E^*}{\sigma_{Y(\varepsilon pre)}}$ monotonically. In addition, it is strongly dependent on $\frac{\sigma_{res}}{\sigma_{Y(\varepsilon pre)}}$. As shown by the solid lines, the data of $\frac{W}{\sigma_{Y(\varepsilon pre)} h_{max}^3}$ were separately approximated by a polynomial function for each $\frac{\sigma_{res}}{\sigma_{Y(\varepsilon pre)}}$ value. The detail approximated function is expressed as follows:

$$\frac{W}{\sigma_{Y(\varepsilon pre)} h_{max}^3} = A_1\left[\ln\left(\frac{E^*}{\sigma_{Y(\varepsilon pre)}}\right)\right]^3 + A_2\left[\ln\left(\frac{E^*}{\sigma_{Y(\varepsilon pre)}}\right)\right]^2$$
$$+ A_3\left[\ln\left(\frac{E^*}{\sigma_{Y(\varepsilon pre)}}\right)\right] + A_4. \qquad (Eq\ 6)$$

The coefficients A_1-A_4 are dependent on $\frac{\sigma_{res}}{\sigma_{Y(\varepsilon pre)}}$, and these, along with the correlation factor R, are shown in Table 2. When these coefficients are interpolated as a function of $\frac{\sigma_{res}}{\sigma_{Y(\varepsilon pre)}}$, Eq 6 at a given $\frac{\sigma_{res}}{\sigma_{Y(\varepsilon pre)}}$ can be deduced. This interpolation of the coefficients A_1-A_4 with $\frac{\sigma_{res}}{\sigma_{Y(\varepsilon pre)}}$ is shown in Fig. 12 in the appendix. Therefore, by substituting the values of W and h_{max} into Eq 6, the relationship between $\frac{E^*}{\sigma_{Y(\varepsilon pre)}}$ and $\frac{\sigma_{res}}{\sigma_{Y(\varepsilon pre)}}$ can be deduced uniquely.

For the unloading, the function $\frac{W_u}{\sigma_{Y(\varepsilon pre)} h_e^3}$ can be deduced by using the parametric FEM data in Eq 5. Figure 7 shows the function of Eq 5, indicating that $\frac{W_u}{\sigma_{Y(\varepsilon pre)} h_e^3}$ is strongly dependent on $\frac{E^*}{\sigma_{Y(\varepsilon pre)}}$. As shown in the enlarged figure, $\frac{W_u}{\sigma_{Y(\varepsilon pre)} h_e^3}$ is slightly dependent on the value of $\frac{\sigma_{res}}{\sigma_{Y(\varepsilon pre)}}$. For each $\frac{\sigma_{res}}{\sigma_{Y(\varepsilon pre)}}$ value, the data of $\frac{W_u}{\sigma_{Y(\varepsilon pre)} h_e^3}$ are approximated by the following polynomial function:

$$\frac{W_u}{\sigma_{Y(\varepsilon pre)} h_e^3} = B_1\left[\ln\left(\frac{E^*}{\sigma_{Y(\varepsilon pre)}}\right)\right]^3 + B_2\left[\ln\left(\frac{E^*}{\sigma_{Y(\varepsilon pre)}}\right)\right]^2$$
$$+ B_3\left[\ln\left(\frac{E^*}{\sigma_{Y(\varepsilon pre)}}\right)\right] + B_4. \qquad (Eq\ 7)$$

The coefficients B_1-B_4 are dependent on $\frac{\sigma_{res}}{\sigma_{Y(\varepsilon pre)}}$, which are shown in Table 3. Similar to Eq 6, by interpolating these

coefficients with $\frac{\sigma_{res}}{\sigma_{Y(\varepsilon pre)}}$, the value of Eq 7 at a given $\frac{\sigma_{res}}{\sigma_{Y(\varepsilon pre)}}$ can be deduced. This interpolation of the coefficients B_1-B_4 with $\frac{\sigma_{res}}{\sigma_{Y(\varepsilon pre)}}$ is also shown in Fig. 13 in the appendix. Therefore, by introducing the values of W_u and h_e into Eq 7, the relationship between $\frac{E^*}{\sigma_{Y(\varepsilon pre)}}$ and $\frac{\sigma_{res}}{\sigma_{Y(\varepsilon pre)}}$ can be deduced uniquely. In conclusion, two independent relationships between $\frac{E^*}{\sigma_{Y(\varepsilon pre)}}$ and $\frac{\sigma_{res}}{\sigma_{Y(\varepsilon pre)}}$ can be obtained from Eq 6 and 7.

4.2 Reverse Analysis Procedure

This section explains the estimation process of our method. An indentation test with a Berkovich indenter was carried out once (referred to as a single indentation test). As shown in Fig. 2(b), we first obtained the indentation responses of the loading curve (W, h_{max}) and the unloading curve (W_u, h_e). The loading data (W, h_{max}) were introduced into Eq 6 and then a relationship between $\frac{E^*}{\sigma_{Y(\varepsilon pre)}}$ and $\frac{\sigma_{res}}{\sigma_{Y(\varepsilon pre)}}$ was obtained. Subsequently, the unloading data (W_u, h_e) were substituted into Eq 7, yielding another relationship between $\frac{E^*}{\sigma_{Y(\varepsilon pre)}}$ and $\frac{\sigma_{res}}{\sigma_{Y(\varepsilon pre)}}$. The reduced modulus E^* is known prior. Thus, two independent relationships between $\frac{E^*}{\sigma_{Y(\varepsilon pre)}}$ and $\frac{\sigma_{res}}{\sigma_{Y(\varepsilon pre)}}$ provide the yield stress $\sigma_{Y(\varepsilon pre)}$ (which further leads to the pre-strain) and residual stress σ_{res}.

Here, we illustrate the reverse analysis process via an example. The example uses an austenitic stainless steel, SUS316L, having a pre-strain of 20% and a residual stress of

161 MPa. The corresponding yield stress is calculated to be 645 MPa from Eq 1, and then the residual stress normalized by yield stress $\frac{\sigma_{res}}{\sigma_{Y(\varepsilon pre)}}$ is calculated to be approximately 0.25. The indentation curve yields the data (W, h_{max}) from the loading curve and (W_u, h_e) from the unloading curve. These data are introduced to the Eq 6 and 7, yielding two relationships between $\frac{E^*}{\sigma_Y}$ and $\frac{\sigma_{res}}{\sigma_{Y(\varepsilon pre)}}$. Figure 8 shows the relationship between $\frac{E^*}{\sigma_{Y(\varepsilon pre)}}$ and $\frac{\sigma_{res}}{\sigma_{Y(\varepsilon pre)}}$ derived from Eq 6 and 7. Their relationships have different slopes. They intersect at the point of $\frac{E^*}{\sigma_{Y(\varepsilon pre)}}$ = 334 and $\frac{\sigma_{res}}{\sigma_{Y(\varepsilon pre)}}$ = 0.23. This is the estimated solution for $\sigma_{Y(\varepsilon pre)}$ = 642 MPa (which corresponds to εpre of 19.8%) and σ_{res} = 148 MPa. As mentioned above, the input value is $\sigma_{Y(\varepsilon pre)}$ = 645 MPa and σ_{res} = 161 MPa, which are close to our estimation. This emphasizes that our method is very simple, since it uses only two dimensionless functions, and yields reliable estimations. The estimation accuracy and robustness of our method will be investigated in the next section.

5. Method Validation

5.1 Numerical Experiment

The method presented was applied to the numerical experiment in order to investigate its estimation accuracy and robustness. As mentioned above, a parametric FEM study was

Table 2   Coefficient of Eq 6 with respect to $\sigma_{res}/\sigma_{Y(\varepsilon pre)}$

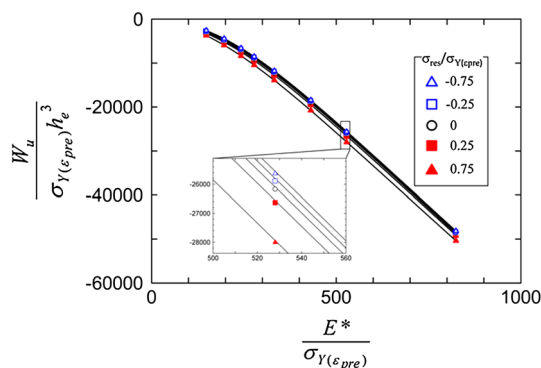| $\sigma_{res}/\sigma_{Y(\varepsilon pre)}$	A_1	A_2	A_3	A_4	$|R|$
−0.75	4.586×10^0	-7.506×10^1	4.171×10^2	-7.518×10^2	0.9998
−0.25	4.325×10^0	-7.072×10^1	3.938×10^2	-7.139×10^2	0.9999
0	4.083×10^0	-6.644×10^1	3.690×10^2	-6.685×10^2	0.9999
0.25	4.001×10^0	-6.489×10^1	3.595×10^2	-6.516×10^2	0.9999
0.75	3.791×10^0	-6.090×10^1	3.347×10^2	-6.060×10^2	0.9999

Fig. 7 Relationship between $\frac{W_u}{\sigma_{Y(\varepsilon pre)} h_e^3}$ and $\frac{E^*}{\sigma_{Y(\varepsilon pre)}}$ at each $\frac{\sigma_{res}}{\sigma_{Y(\varepsilon pre)}}$
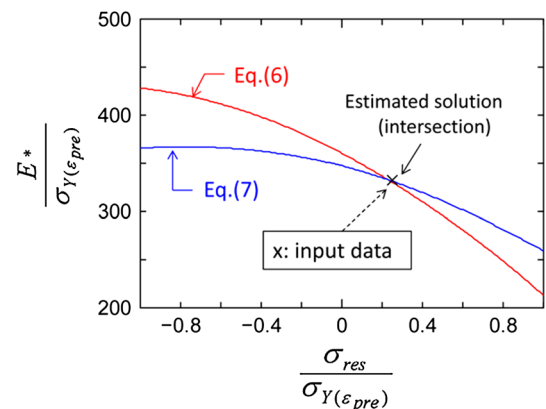

Fig. 8 Identification of the estimated solution as being the intersection of the two curves (from Eq 6 and 7)

Table 3   Coefficient of Eq 7 with respect to $\sigma_{res}/\sigma_{Y(\varepsilon pre)}$

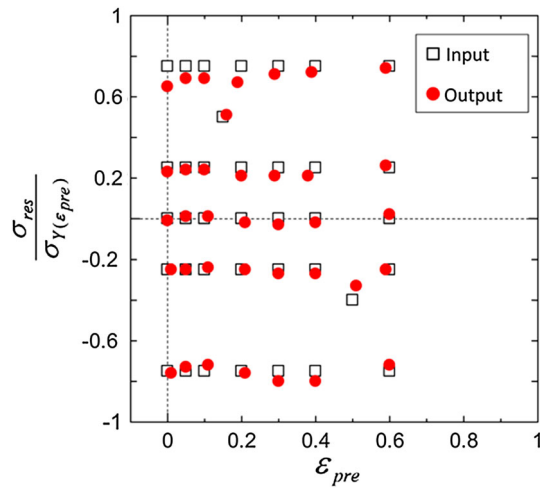| $\sigma_{res}/\sigma_{Y(\varepsilon pre)}$	B_1	B_2	B_3	B_4	$|R|$
−0.75	-5.125×10^3	7.309×10^4	-3.515×10^5	5.685×10^5	0.9999
−0.25	-5.252×10^3	7.527×10^4	-3.640×10^5	5.917×10^5	0.9999
0	-5.257×10^3	7.547×10^4	-3.659×10^5	5.968×10^5	0.9999
0.25	-5.153×10^3	7.384×10^4	-3.576×10^5	5.829×10^5	0.9999
0.75	-4.830×10^3	6.860×10^4	-3.302×10^5	5.359×10^5	0.9999

Fig. 9 Comparison of the estimated result by reverse analysis with input values

Table 4 Representative materials for sensitivity analysis

	Case1	Case2	Case3	Case4
$\sigma_{res}/\sigma_{Y(\varepsilon pre)}$	−0.4	0.25	−0.25	0.75
ε_{pre}	0.5	0.4	0.1	0.2

carried out to establish the dimensionless function, and those data were employed to estimate the residual stress and prestrain. Furthermore, two additional sets ($\varepsilon_{pre} = 0.15$, $\frac{\sigma_{res}}{\sigma_{Y(\varepsilon pre)}} = 0.5$ and $\varepsilon_{pre} = 0.5$ $\frac{\sigma_{res}}{\sigma_{Y(\varepsilon pre)}} = -0.4$) were also investigated to verify the method. Note that these two material cases were not included in the FEM parametric study (to establish the dimensionless function of Eq 6 and 7). For all cases, we extracted the loading (W, h_{max}) and unloading data (W_u, h_e) from the computational indentation curve, and then estimated the values of ε_{pre} and σ_{res}.

The estimated values of (ε_{pre}, $\frac{\sigma_{res}}{\sigma_{Y(\varepsilon pre)}}$) by the method are shown in Fig. 9. The squares indicate the input values (solutions), and the circles denote the estimates. All calculated results agree with the input data, with an error of less than about 20%, which is similar to that of a previously developed estimation method of elastoplastic properties with reverse analysis (Ref 10, 11, 14, 30). This indicates that the present algorithm is fairly reliable and has satisfactory accuracy. Note that the reverse analysis of Fig. 9 can uniquely estimate the input data, indicating that there is no uniqueness issue for the present input cases.

Another concern for experimental estimations is the perturbation of indentation response. When we experimentally conduct an indentation test in a laboratory, uncertainties in the experimental indentation responses are usually inevitable due to several factors related to the material and indentation measurement equipment. A number of previous studies have investigated the robustness of the method, which is a key issue for accuracy. In other words, it is important to investigate the sensitivity of the determined properties to variations in the input data, and to clarify how scatter in the input data affects these properties. In this study, we conducted a sensitivity analysis for four representative materials (Table 4). For the indentation curve (i.e., indentation work volume and depth), the perturbations were set to 2%, since previous studies have used

Table 5 Case study for sensitivity analysis of representative materials
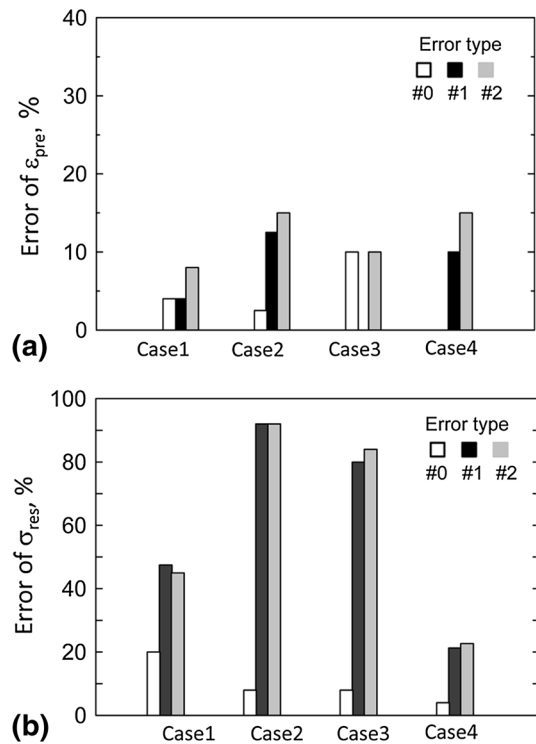
Case study	Error of W, %	Error of W_u, %
#0	0	0
#1	+2	0
#2	0	+2

Fig. 10 Sensitivity study of the representative materials; (a) prestrain ε_{pre}, and (b) residual stress σ_{res}

this value for sensitivity analyses (Ref 26). These perturbation cases (#0, #1. #2) are shown in Table 5.

The deviations (errors in the estimated values compared to the input values) in the absolute values are shown in Fig. 10(a) and (b) for the pre-strain ε_{pre} and the residual stress σ_{res}, respectively. Values of ε_{pre} (Fig. 10a) show good agreement and robustness for all perturbation cases. On the contrary, values of σ_{res} show large errors for the perturbation cases. This is because the dependency of σ_{res} on the indentation curve is smaller than that of ε_{pre} as shown in Fig. 5. Thus, the estimation of σ_{res} may be more sensitive on measurement error. Several previous studies on sensitivity analyses reported that their methods induced 50 % error maximum (Ref 26). This indicates that the present method may relatively underperform in the presence of perturbations due to potential experimental errors, but these error cases (Table 5) may represent extreme examples. The actual experimental situation is addressed in the next section.

5.2 Experimental Investigation

5.2.1 Experimental Setup. This study used micro indentation equipment (Dynamic Ultra-micro Hardness Tester DUH-501, Shimadzu corp.). A Berkovich indenter was also employed. The loading rate was set to 28 mN/s. The maximum indentation force was set to 1962 mN.

Table 6 Experimental verification of cold-rolled and shot-peened SUS316L, showing the comparison of between the estimations (σ_{res} and ε_{pre}) from the present indentation method and those of experimental data (obtained from x-ray diffraction and uniaxial tensile test)

Material	Solution (a)		Estimation	
	ε_{pre}	σ_{res}, MPa	ε_{pre}	σ_{res}, MPa
Mat. 1 (AR)	0	0	0	8
Mat. 2 (CR-5%)	0.042	0	0.039	−11
Mat. 3 (CR-10%)	0.089	0	0.103	15
Mat. 4 (CR-20%)	0.199	0	0.202	−32
Mat. 5 (SP)	Unknown	−450 ± 138	0.444	−494

(a) "Solution" is the material property obtained from the experiment. For Mat. 2-4 of cold-rolled steel (CR), the pre-strain ε_{pre} was obtained by tensile test. For Mat. 5 of shot-peened steel (SP), the residual stress was measured by x-ray diffraction

The specimen utilized was austenitic stainless steel, which is commercially available SUS316L. This study prepared several SUS316L steels having different pre-strain and residual stress values. For a pre-strained steel, we used cold-rolled (CR) SUS316L, which is commercially available. The rolling ratio was with 5, 10, and 20% strain. These steels were designated as Mat. 1, 2, 3, and 4. Note that Mat. 1 was the as-received (AR) virgin SUS316L. Their properties are shown in Table 6. We also conducted a uniaxial tensile test to obtain the stress-strain curves of cold-rolled steels (Mat. 2-4). By comparing the curve with that of the as-received steel, the values of pre-strain ε_{pre} were obtained (see Table 6).

Meanwhile, a residual stress was introduced via shot peening (SP), which utilized a zirconia ball that had a diameter of 0.6 mm. During peening, the shot pressure was set to 0.45 MPa. After peening, we mechanically polished the peening surface to obtain a smooth surface (where indentation test was applicable). The residual stress of the polished surface was measured based on the $\sin^2\psi$ method using the x-ray diffraction system PSPC-MSF-3M (Rigaku Corporation). We used the x-ray diffraction method to measure the x-ray diffraction. The x-ray source was Cr-Kα, which operated at 35 kV and 8 mA. The diffractive plane was (220) γ-Fe, and the reference diffractive angle 2θ was approximately 130°. The stress factor for the x-ray diffraction was −624.68 MPa/°. Three different points on the surface were selected for the measurement. For each point, the measurements were conducted from the orthogonal axis of two directions. The averaged datum for one direction was $\sigma_{res} = −507 ± 165$ MPa, and that for other direction was −392 ± 104 MPa. Although this result shows a relatively large scatter (due to a mechanically polished condition), the stresses along two orthogonal axes were the same, indicating that the specimen surface experienced in-plane equi-biaxial compressive residual stresses[‡]. Therefore, the averaged σ_{res} was −450 ± 138 MPa.

5.2.2 Experimental Results. Figure 11 shows the indentation curves of sheets that underwent cold rolling and shot peening (as shown in Table 6). Each test was carried out more than ten times, and the curves represent the averaged values. In Fig. 11, the indentation depth became shallower with the increase in the cold-rolled ratio. In addition, the shot peening steel was found to be the hardest material. By using our approach, the pre-strain ε_{pre} and residual stress σ_{res} were
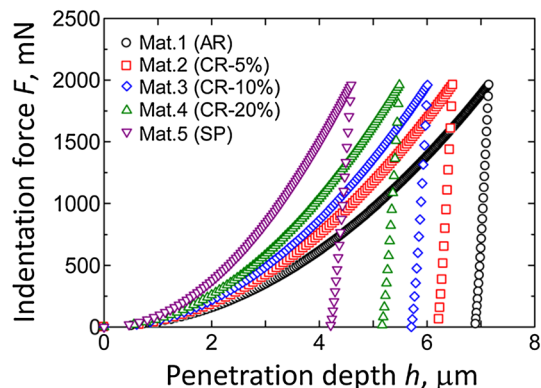

Fig. 11 Indentation curves of SUS316L with cold rolling process and shot peening treatment

estimated as shown in Table 6. The virgin steel and cold-rolled steel (Mat. 1-4) show a good estimation of ε_{pre}. However, the residual stress of cold-rolled steel was not investigated, and the stress on the surface may be very small since the distribution of Vickers hardness in the transverse section is almost constant[§]. Therefore, we described σ_{res} of zero as in Table 6, indicating that the estimation of σ_{res} also showed good agreement. Finally, the shot peening steel (Mat. 5) was investigated. The estimation of σ_{res} was −494 MPa, which agrees well with the measurement data (−450 MPa). The ε_{pre} was estimated to be 0.444, suggesting that a large plastic strain was introduced. Although this value is not known for the actual property, it was validated as follows. It is reported that the Vickers hardness of present peening steel archives HV = 400 (Ref 31), which is quite larger than that of the as-received steel (HV = 150). Using the Tabor relationship (Ref 6), the corresponding yield stress (plastic flow stress) was approximately 1.3 GPa, which favorably compares with 0.9 GPa (when the $\varepsilon_{pre} = 0.444$ was substituted into Eq 1). Thus, our present method can apply to SUS316L having pre-strain and residual stress.

As mentioned in the Introduction, most previous studies for measuring the residual stress require a reference sample with a stress-free state, and investigated how the indentation response

[‡]The shot peening method may not theoretically induce equi-biaxial stress condition on a specimen surface. However, the difference in residual stresses along each direction is less than 30%. It is thus assumed that the residual stress develops in-plane equi-biaxially.

[§]Micro Vickers hardness tests were carried out in the transverse section of the CR specimen, indicating the constant hardness (i.e., no gradient of hardness through the thickness). It is suggested that the present cold-rolled method induces plastic strain homogeneously in the transverse section. Thus, the residual stress is very small.
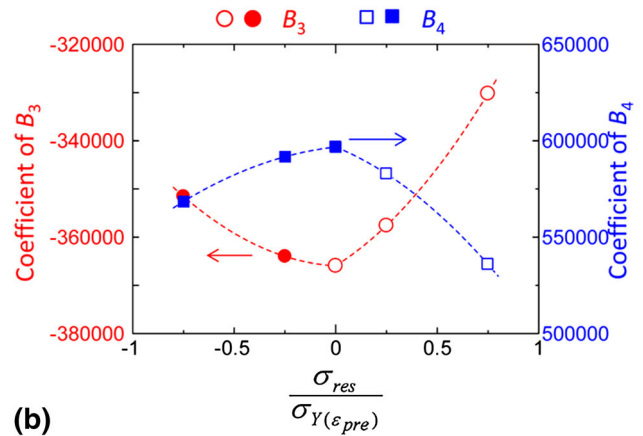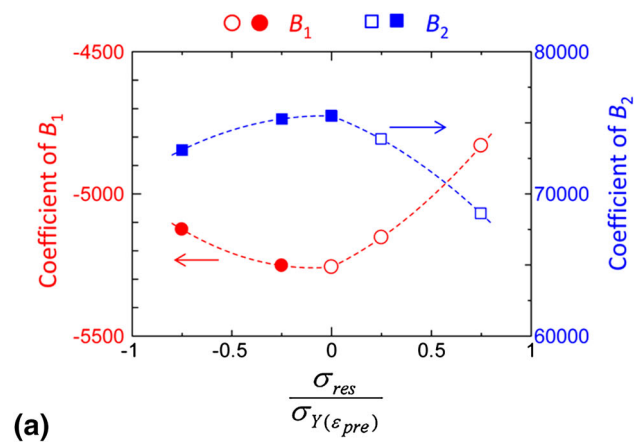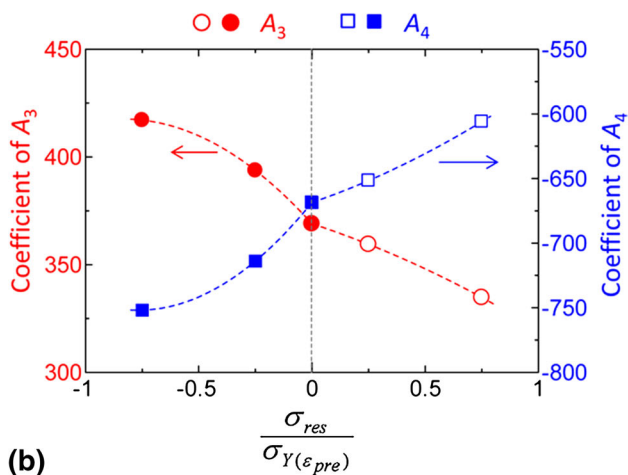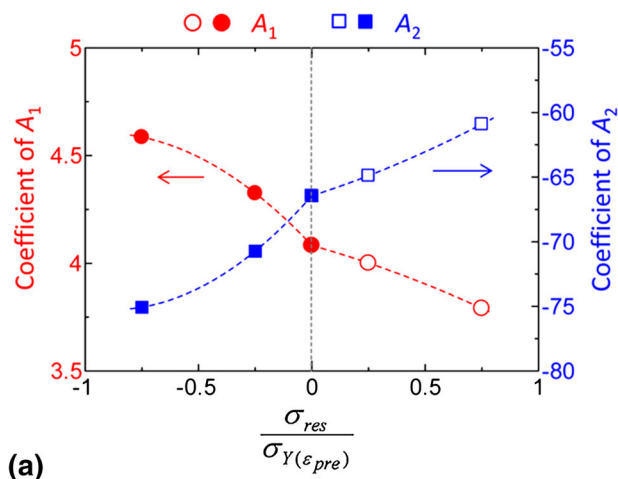
Fig. 12 Coefficients of Eq 6 with respect to $\frac{\sigma_{res}}{\sigma_{Y(\varepsilon_{pre})}}$

Fig. 13 Coefficients of Eq 7 with respect to $\frac{\sigma_{res}}{\sigma_{Y(\varepsilon_{pre})}}$

Table 7 Coefficient of Eq. A1

	$\sigma_{res}/\sigma_{Y(\varepsilon pre)} \leq 0$			$\sigma_{res}/\sigma_{Y(\varepsilon pre)} \geq 0$		
	a	b	c	a	b	c
A_1	$-5.9970480e{-}1$	-1.1201870	4.0828625	$-1.2479867e{-}1$	$-2.9542033e{-}1$	4.0828625
A_2	$1.1271768e{+}1$	$1.9951050e{+}1$	$-6.6440609e{+}1$	2.3472507	5.6265833	$-6.6440609e{+}1$
A_3	$-6.9895973e{+}1$	$-1.1661859e{+}2$	$3.6899038e{+}2$	$-1.5061040e{+}1$	$-3.4307660e{+}1$	$3.6899038e{+}2$
A_4	$1.4048624e{+}2$	$2.1641652e{+}2$	$-6.6853446e{+}2$	$3.1174613e{+}1$	$6.0031187e{+}1$	$-6.6853446e{+}2$
B_1	$3.1368667e{+}2$	$5.8862067e{+}1$	$-5.2571137e{+}3$	$3.0531147e{+}2$	$3.3998653e{+}2$	$-5.2571137e{+}3$
B_2	$-4.7461733e{+}3$	$-3.7353133e{+}2$	$7.5479003e{+}4$	$-5.1811093e{+}3$	$-5.2780587e{+}3$	$7.5479003e{+}4$
B_3	$2.2884853e{+}4$	$-2.0091067e{+}3$	$-3.6592774e{+}5$	$2.8424133e{+}4$	$2.6326447e{+}4$	$-3.6592774e{+}5$
B_4	$-3.5108773e{+}4$	$1.1389567e{+}4$	$5.9677873e{+}5$	$-5.0981947e{+}4$	$-4.2944393e{+}4$	$5.9677873e{+}5$

was changed by residual stress (Ref 22). However, the present study does not require a stress-free sample as reference, and it can estimate both residual stress and yield stress (with respect to pre-strain) simultaneously. It is also emphasized that our method follows a very simple framework, since it only needs two dimensionless functions with simple polynomial equations. Although the present method is applicable to only an austenitic stainless steel that obeys the Ludwick's work hardening law and involves in-plane equi-biaxial residual stress, it may also be applicable to any other material using a similar concept. Such work will be addressed in the future.

6. Conclusion

This study proposed a new indentation method to simultaneously evaluate the residual stress and plastic strain of an austenitic stainless steel. This method focuses on an austenitic stainless steel, SUS316L, which obeys the Ludwick's work hardening law and involves in-plane equi-biaxial residual stress. Note that the framework is applicable to any material with little modification. A Berkovich indenter penetrates the steel until it undergoes full plastic deformation, and then the

indentation curve, which represents the relationship between indentation force and penetration depth, is obtained. The parameter from the curve is used for a reverse analysis in order to estimate residual stress and plastic strain.

Comprehensive numerical experiments with FEM were first carried out in order to simulate a Berkovich indentation test for SUS316L having various plastic strain (pre-strain) and residual stress values. It was found that the indentation force increases with the increase in the pre-strain as well as compressive residual stress. Next, to establish the reverse analysis, the parametric FEM study by changing the residual stress σ_{res} and pre-strain ε_{pre} was conducted, such that we deduced the relationship between the indentation curve and the parameters ε_{pre} and σ_{res} for the dimensionless function. In particular, the indentation total work W from the loading curve and elastic work W_u from the unloading curve were employed as the parameter for the proposed reverse analysis. In fact, this relationship can be expressed by only two dimensionless functions with relatively simple formulae. Thus, by substituting the indentation curve (indentation work of W and W_u) into the functions, the present method could estimate both ε_{pre} and σ_{res} readily.

The robustness of our method was verified by error estimation against input perturbations using numerical studies. In parallel, laboratory experiments were conducted in order to estimate the plastic strain and residual stress based on the proposed framework. Microindentation tests were conducted for several SUS316L steels, which were as-received steel, pre-strained steel (cold-rolled steel), and peening steel with residual stress. It was revealed that the proposed indentation technique could reasonably and quantitatively evaluate both pre-strain and residual stress. Since the indentation method can evaluate local mechanical properties, our method may be useful for a complex material system, such as welded steel, plastic worked steel, pipe, and mechanical component/structures of SUS316L.

Appendix

This section describes the coefficient of Eq 6 and 7 as shown in Fig. 12 and 13. For all figures, the data are approximated by a quadratic function as indicated by the dotted line. Note that at the boundary of $\frac{\sigma_{res}}{\sigma_{Y(\varepsilon pre)}} = 0$, we separately approximated data by the function of Eq A1. The quadratic function is given as follows:

$$A_i \text{ or } B_i = a\left(\frac{\sigma_{res}}{\sigma_{Y(\varepsilon pre)}}\right)^2 + b\left(\frac{\sigma_{res}}{\sigma_{Y(\varepsilon pre)}}\right) + c \quad (i = 1-4)$$

$$\text{(Eq A1)}$$

This function involves three coefficients, namely a, b, and c, and are listed in Table 7. At the boundary of $\frac{\sigma_{res}}{\sigma_{Y(\varepsilon pre)}} = 0$, these

are different for all A_i and B_i ($i = 1\text{-}4$). By using Table 7 and Eq A1, the coefficients of A_i and B_i ($i = 1\text{-}4$) can be obtained for any $\frac{\sigma_{res}}{\sigma_{Y(\varepsilon pre)}}$ value. Thus, the dimensionless functions of Eq 6 and 7 for any $\frac{\sigma_{res}}{\sigma_{Y(\varepsilon pre)}}$ value can be established.

References

1. M.D. Giorgi, Residual Stress Evolution in Cold-Rolled Steels, *Int. J. Fatigue*, 2011, **33**, p 507–512
2. R.B. Cruise and L. Gardner, Residual Stress Analysis of Structural Stainless Steel Sections, *J. Constr. Steel Res.*, 2008, **64**, p 352–366
3. K.H. Lo, C.H. Shek, and J.K.L. Lai, Recent Developments in Stainless Steels, *Mater. Sci. Eng. R*, 2009, **65**, p 39–104
4. A. Yonezu, H. Cho, and M. Takemoto, Monitoring of Stress Corrosion Cracking in Stainless Steel Weldments by Acoustic and Electrochemical Measurement, *Meas. Sci. Technol.*, 2006, **17**, p 2447–2454
5. J. Lu, M. James, and L. Mordfin, *Handbook of Measurement of Residual Stresses*, Fairmont Press, Lilburn, GA, 1996
6. D. Tabor, *Hardness of Metals*, Oxford University Press, Oxford, 1951
7. W.C. Oliver and G.M. Pharr, An Improved Technique for Determining Hardness and Elastic-Modulus Using Load and Displacement Sensing Indentation Experiments, *J. Mater. Res.*, 1992, **7**, p 1564–1583
8. M. Dao, N. Chollacoop, K.J. VanVliet et al., Computational Modeling of the Forward and Reverse Problems in Instrumented Sharp Indentation, *Acta Mater.*, 2001, **49**, p 3899–3918
9. N. Ogasawara, N. Chiba, and X. Chen, A Simple Framework of Spherical Indentation for Measuring Elastoplastic Properties, *Mech. Mater.*, 2009, **41**, p 1025–1033
10. A. Yonezu, K. Yoneda, H. Hirakata et al., A Simple Method to Evaluate Anisotropic Plastic Properties Based on Dimensionless Function of Single Spherical Indentation—Application to SiC Whisker Reinforced Aluminum Alloy, *Mater. Sci. Eng. A*, 2010, **527**, p 7646–7657
11. Y.P. Cao and J. Lu, Depth-sensing Instrumented Indentation with Dual Sharp Indenters: Stability Analysis and Corresponding Regularization Schemes, *Acta Mater.*, 2004, **52**, p 1143–1153
12. Y.T. Cheng and C.M. Cheng, Scaling, Dimensional Analysis, and Indentation Measurements, *Mater. Sci. Eng.*, 2004, **R44**, p 91–149
13. X. Chen, N. Ogasawara, M. Zhao, and N. Chiba, On the Uniqueness of Measuring Elastoplastic Properties from Indentation: The Indistinguishable Mystical Materials, *J. Mech. Phys. Solids*, 2007, **55**, p 1618–1660
14. A. Yonezu, H. Akimoto, S. Fujisawa, and X. Chen, Spherical Indentation Method for Measuring Local Mechanical Properties of Welded Stainless Steel at High Temperature, *Mater. Des.*, 2013, **52**, p 812–820
15. S. Matsuoka, Relationship Between 0.2% Proof Stress and Vickers Hardness of Work-Hardened Low Carbon Austenitic Stainless Steel, 316SS, *Jpn. Soc. Mech. Eng. A*, 2004, **70**, p 1535–1541
16. Y. Estrin and A. Vinogradov, Extreme Grain Refinement by Severe Plastic Deformation: A Wealth of Challenging Science, *Acta Mater.*, 2013, **61**, p 782–817
17. T. Ohno and T. Ogawa, Study on Plastic Deformation and Hardening Mechanism of Austenitic Stainless Steels at Room and Cryogenic Temperatures, *Jpn. Soc. Mech. Eng. A*, 2007, **3**, p 338–344
18. S. Suresh and A.E. Giannakopoulos, A New Method for Estimating Residual Stresses by Instrumented Sharp Indentation, *Acta Mater.*, 1998, **46**, p 5755–5767
19. T.Y. Tsui, W.C. Oliver, and G.M. Pharr, Influences of Stress on the Measurement of Mechanical Properties Using Nanoindentation 1. Experimental Studies in an Aluminum Alloy, *J. Mater. Res.*, 1996, **11**, p 752–759
20. J.G. Swadener, B. Taljat, and G.M. Pharr, Measurement of Residual Stress by Load and Depth Sensing Indentation with Spherical Indenters, *J. Mater. Res.*, 2001, **16**, p 2091–2102
21. B. Xu and Z. Yue, Study of the Ratcheting by the Indentation Fatigue Method with a Flat Cylindrical Indenter: Part I. Finite Element Simulation, *J. Mater. Res.*, 2006, **22**, p 186–191
22. Jang J-i, Estimation of Residual Stress by Instrumented Indentation: A Review, *J. Ceram. Process. Res.*, 2009, **10**, p 391–400
23. M. Bocciarelli and G. Maier, Indentation and Imprint Mapping Method for Identification of Residual Stresses, *Comput. Mater. Sci.*, 2007, **39**, p 381–392

24. M. Nishikawa and H. Soyama, Two-step Method to Evaluate Equibiaxial Residual Stress of Metal Surface Based on Micro-indentation Tests, *Mater. Des.*, 2011, **32**, p 3240–3247

25. X. Chen, J. Yan, and A.M. Karlsson, On the Determination of Residual Stress and Mechanical Properties by Indentation, *Mater. Sci. Eng. A*, 2006, **416**, p 139–149

26. M. Zhao, X. Chen, J. Yan, and A.M. Karlsson, Determination of Uniaxial Residual Stress and Mechanical Properties by Instrumented Indentation, *Acta Mater.*, 2006, **54**, p 2823–2832

27. Marc. Marc 2011, Theory and User's Manual A 2011

28. F.P. Bowden and D. Tabor, *The Friction and Lubrications of Solids*, Oxford University Press, Oxford, 1950

29. Y.T. Cheng and C.M. Cheng, Scaling Approach to Conical Indentation in Elastic-Plastic Solids with Work Hardening, *J. Appl. Phys.*, 1998, **84**, p 1284–1291

30. M.-Q. Le, Material Characterization by Dual Sharp Indenters, *Int. J. Solids Structures*, 2009, **46**, p 2988–2998

31. Takemoto M. Personal communication. 2013